Reactions $K^-p \to \Sigma^0\pi^0$ and $K^-p \to \Lambda\pi^0$ in the momentum range 240 to 450 MeV/c *

T. S. Mast, M. Alston-Garnjost, R. O. Bangerter, A. S. Barbaro-Galtieri, F. T. Solmitz, and R. D. Tripp
Lawrence Berkeley Laboratory, University of California, Berkeley, California 94720
(Received 9 December 1974)

An analysis has been made of 57 600 events of the type $K^-p \to \Lambda$ + missing neutrals obtained in the Berkeley 25-in. hydrogen bubble chamber. The data were divided into intervals of 10 MeV/c in incident momentum and fits were made to the distribution in missing neutral mass, the production cosine, and the polarization of the Λ. These fits yielded Legendre coefficients describing the cross sections and polarizations for $K^-p \to \Sigma^0\pi^0$ and $K^-p \to \Lambda\pi^0$ in the momentum range 240 to 450 MeV/c. The cross sections and polarization in the $\Sigma^0\pi^0$ final state show marked structure coming from the production and decay of $\Lambda(1520)$. The cross sections and polarizations for the $\Lambda\pi^0$ final state vary slowly. No new structure is observed.

I. INTRODUCTION

In the region near 400 MeV/c incident momentum the major structure in the K^-p channel is the $\Lambda(1520)$.[1] As part of a detailed study of all the final states in this region[2] we report here on the $\Sigma^0\pi^0$ and $\Lambda\pi^0$ final states. Data on the $\Sigma^0\pi^0$ final state coupled with the forthcoming $\Sigma^\pm\pi^\mp$ data provide a test of charge independence[3] and a strong constraint on partial-wave analyses in this region. The $\Lambda\pi^0$ final state is pure $I=1$ and the $\Sigma^0\pi^0$ final state is pure $I=0$.

A sample of 57 600 events of the type $K^-p \to \Lambda$ + neutrals was obtained in the Berkeley 25-in. hydrogen bubble chamber. In Sec. II we describe the experimental procedures and the bias corrections applied to the data. In Sec. III a qualitative description of the data is given. At the low momenta considered here there is appreciable overlap of the $\Sigma^0\pi^0$ and $\Lambda\pi^0$ contributions to the observed missing neutral mass spectrum. Contributions to the data from other final states (primarily $\Lambda\pi^0\pi^0$) further complicate the extraction of the cross sections and polarizations of the individual $\Sigma^0\pi^0$ and $\Lambda\pi^0$ final states. Section IV describes the event-by-event maximum-likelihood fit used to extract Legendre polynomial expansion coefficients that describe the angular distributions and polarizations for the individual final states. Section V summarizes the results of this fit and presents our conclusions. The Appendix explains the formulas used to derive the Σ^0 production distribution and polarization from those of its decay Λ.

II. EXPERIMENTAL PROCEDURES

From an exposure of the Berkeley 25-in. hydrogen bubble chamber to a K^- beam we have obtained 1.3×10^6 pictures. The beam has been fully described elsewhere.[4] Typically, each picture contained six K^- tracks and two background tracks. The background consisted of pions, muons, and some electrons. Background tracks had close to minimum ionization and were thus easily distinguished from the K^- tracks, which at our momentum have about three times minimum ionization.

By movement of the target and by use of a beryllium beam degrader, we were able to obtain K^- momenta between 240 and 450 MeV/c. The data were taken with 24 different beam settings. However, most of the pathlength (Fig. 1) occurs close to 395 MeV/c, the momentum required to form $\Lambda(1520)$.[5]

The film was scanned for all topologies including those with a zero prong and vee. On the basis of ionization, the scanners distinguished between vees from the decay $K^0 \to \pi^+\pi^-$ and those from the

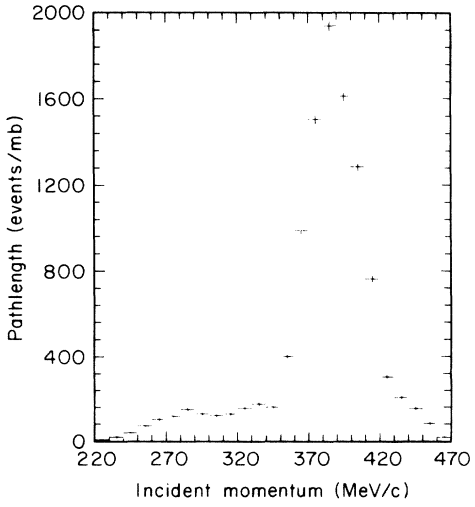

FIG. 1. Pathlength (events/mb) versus incident K^- momentum (MeV/c).

decay $\Lambda \to p\pi^0$. All of the film was scanned once, 38% was scanned twice, and 7% was scanned three times. All events within a restricted fiducial volume were measured with the Spiral Reader or Franckenstein measuring projectors. The kinematic reconstruction and fits to reaction hypotheses were performed with the programs TVGP and SQUAW. The vee for events scanned as $\overline{K}^0$ (Λ) was first fitted to the decay $\overline{K}^0 \to \pi^+\pi^-$ ($\Lambda \to p\pi^0$). The incident beam primary interaction point was used to determine the direction of the neutral, making this a three-constraint fit. If the fit to the scanned decay failed, then the fit to the other two-body vee decay was tried. If both failed then fits to three-body $\overline{K}^0$ decays were tried. Those events which passed three-constraint decay fits were then fitted to the appropriate production and decay

$$K^-p \to \overline{K}^0 n, \quad \overline{K}^0 \to \pi^+\pi^-, \tag{1}$$

$$K^-p \to \Lambda + \text{missing mass}, \quad \Lambda \to p\pi^0. \tag{2}$$

Events which failed to fit any reaction hypothesis were remeasured until 94% of those scanned as K^0 and 96% of those scanned as Λ passed. The remaining events were generally unmeasurable due to obscuration of a track or the presence of a very short track.

Of those events scanned as $\overline{K}^0$, 6.1% had a better confidence level for a fit to the Λ production and decay. Of those scanned as Λ, 1.4% had a better fit to the $\overline{K}^0$ production and decay.

Only those events which had a confidence level greater than 0.01 were accepted for further analysis. This sample included 29109 events which fitted only reaction (1), 70815 events which fitted only reaction (2), and 824 events which fitted both reactions. Comparison of the confidence levels for those events fitting both reactions showed that in most cases one of the two fits was much preferred. An ambiguous event was considered to be the preferred reaction if the confidence level ratio for the fits was greater than 5.0. Reexamination of a sample of these events showed this to be a good criterion. Of the 824 events 82 were accepted as $\overline{K}^0$ events and 712 as Λ events. The remaining truly ambiguous 30 events, being a negligible number, were simply eliminated from the sample.

To ensure sufficient track lengths for a good measurement of the Λ momentum, further restrictions were made on the fiducial volumes for the production and decay vertices. These reduced the sample of Λ events to 63794 events. To correct for a scanning loss of short-length Λ's, all events with a projected length less than 2.5 mm in space were eliminated and the remaining 57880 events were weighted to account for the cut. The weighting also accounted for loss due to escape from the decay vertex fiducial volume. The mean weight was 1.23. Further losses were investigated by looking at the distribution of the decay proton in the Λ rest frame. Anisotropy in this distribution was found coming from the loss of events with short-length protons and events with the Λ vee seen edge-on by the scanners. This anisotropy was removed by rejecting events with a proton length less than 3 mm in space and weighting the remaining events. This reduced the sample to 56748 events with a mean weight of 1.34.

The lifetime distribution of the final sample is shown in Fig. 2. In order to remove the effect of the cut on short-length Λ's, the events have been plotted as a function of $(t - t_0)$ in units of the known Λ lifetime (τ_Λ). For each event, t_0 is given by 2.5 mm/($\eta c \tau_\Lambda \cos\lambda$), where η is the ratio of the Λ momentum to its mass and λ is the dip angle. This distribution is consistent with the line corresponding to the known lifetime ($\tau_\Lambda = 2.5 \times 10^{-10}$ sec). The depletion at large lifetimes comes from the escape of the Λ's from the chamber.

The cross section for the reaction was determined from a pathlength based on the τ decays of the beam. The analysis of these τ's has been described in a previous publication.[6] The numbers of both τ's and Λ + missing mass events were corrected for unobserved decay modes and for scanning efficiencies.

The scanning efficiencies were determined from the multiple scans using an extension of the method developed by Derenzo and Hildebrand.[7] The analysis accounts for the differing visibility of events by parameterizing a visibility function $f(v)$, the fraction of the sample seen with an efficiency v, where v varies from 0.0 to 1.0. The extension used for this experiment defines a different visi-

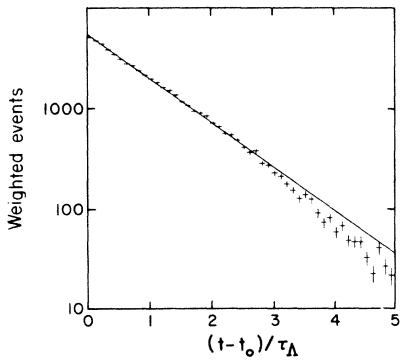

FIG. 2. Distribution of Λ lifetimes shifted by the cut imposed to remove the effect of the loss of short-length Λ's. The depletion at large lifetimes comes from the escape of the Λ's from the chamber.

bility (v_1, v_2, and v_3) for each of the three scans to allow different efficiencies for each scan. The events found on each of the scans were fitted to determine the parameters of the function $f(v_1, v_2, v_3)$, which is then used to calculate the efficiencies. Details of this analysis can be found in Ref. 8. The over-all scanning efficiency was 0.96.

III. DATA

The measured cross section for all Λ + neutrals is shown in Fig. 3. It falls from about 17 mb near 225 MeV/c to about 7 mb near 450 MeV/c. There is a 7 mb peak around 390 MeV/c from $\Lambda(1520)$. There are eight reactions which contribute to this cross section:

1. $K^-p \to \Lambda\pi^0$,
2. $K^-p \to \Sigma^0\pi^0$, $\Sigma^0 \to \Lambda\gamma$
3. $K^-p \to \Lambda\pi^0\pi^0$,
4. $K^-p \to \Lambda\gamma$,
5. $K^-p \to \Sigma^0\gamma$, $\Sigma^0 \to \Lambda\gamma$
6. $K^-p \to \Lambda\pi^0\gamma$,
7. $K^-p \to \Sigma^0\pi^0\gamma$, $\Sigma^0 \to \Lambda\gamma$
8. $K^-p \to \Sigma^0\pi^0\pi^0$, $\Sigma^0 \to \Lambda\gamma$.

In this paper results for the first three channels will be presented. The $\Lambda\gamma$ channel has previously been measured.[9] The $\Sigma^0\gamma$ channel is deduced from the $\Lambda\gamma$ channel by symmetry arguments, while the last three channels are expected to be negligible.

Since only the Λ in each of these final states is observed the data at each incident momentum yield a distribution in three variables:

(i) μ^2, the invariant mass squared of the missing neutrals. This is related to the center-of-mass energy of the Λ as follows:

$$\mu^2 = E_{\text{c.m.}}{}^2 - 2E_{\text{c.m.}}E_\Lambda + m_\Lambda{}^2 .$$

(ii) $\cos\theta$, the cosine of the angle between the missing mass and the K^- in the K^-p center-of-mass system.

(iii) $\cos\beta$, the cosine of the angle between the decay proton of the Λ and the normal to the missing-mass production plane,

$$\cos\beta = \frac{\hat{p}\cdot(\vec{K}\times\vec{\mu})}{|\vec{K}\times\vec{\mu}|},$$

where $\vec{K}$ and $\vec{\mu}$ are the beam and missing-mass directions, and the unit vector $\hat{p}$ is the proton direction in the Λ rest frame.

A schematic diagram of the distributions in the invariant mass squared, μ^2, expected from the above reactions at 395 MeV/c incident momentum is shown in Fig. 4. The relative normalizations here are arbitrary and perfect mass resolution has been assumed. The $\Lambda\pi^0$ and $\Lambda\gamma$ final states contribute at single missing masses. It can be

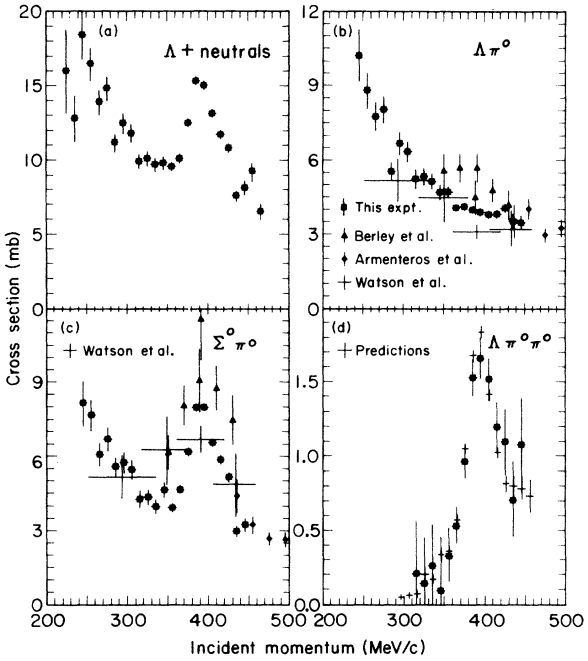

FIG. 3. (a) Cross section (mb) for the reaction $K^-p \to \Lambda$ + missing neutrals as a function of incident K^- momentum (MeV/c). (b), (c), and (d) cross sections (mb) for the $\Lambda\pi^0$, $\Sigma\pi^0$, and $\Lambda\pi^0\pi^0$ final states derived from the fits described in the text. The data of Berley *et al.* (Ref. 13), Armenteros *et al.* (Ref. 14), and Watson *et al.* (Ref. 1) are shown for comparison. The data shown with vertical lines in Fig. 3(d) are predictions based on isotopic spin invariance and the $\Lambda\pi^+\pi^-$ cross sections measured from the same bubble-chamber exposure.

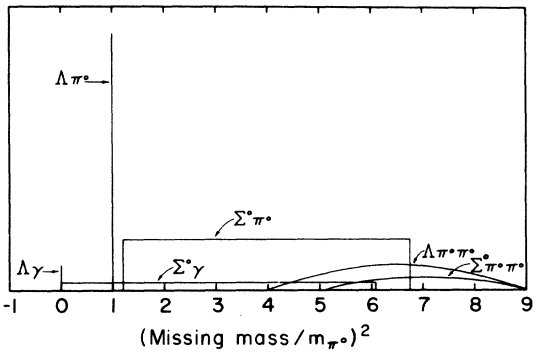

FIG. 4. Schematic diagram of the distributions in missing mass squared ($K^-p \to \Lambda$ + missing mass) expected from different final states at 395 MeV/c. The vertical scale and relative normalizations are arbitrary.

shown that $\Sigma^0\pi^0$ and $\Sigma^0\gamma$ final states contribute rectangular distributions with upper and lower limits that vary slowly with incident momentum. The three-body final states are illustrated as smooth distributions corresponding to projections of uniformly populated Dalitz plots.

Measurement errors naturally lead to finite resolution and an example of the measured missing-mass distribution is shown in Fig. 5. Here the data for all values of $\cos\theta$ and $\cos\beta$ are plotted for the incident momentum interval 390 to 400 MeV/c. The program SQUAW calculates an error for μ^2 for each event, $\delta(\mu^2)$, and this error has been used in the fits described below. The size of this error depends strongly on whether the proton comes to rest and its momentum is determined from range, or whether it leaves the chamber and its momentum is determined from curvature. Those events for which the proton momentum was determined from range have $\delta(\mu^2)$ between 0.06 and 0.20 in units of $m_{\pi^0}{}^2$. If the proton momentum was determined from curvature, then $\delta(\mu^2)$ ranges from 0.1 to 1.0, depending on the length of the track. Since $\delta(\mu^2)$ depends on the length of the proton track available for measurement, it is a function of both the energy (and therefore μ^2) and the production cosine of the Λ.

The variation of $\delta(\mu^2)$ and the different production distributions of the different reactions lead to very different mass spectra for various production angles. Figure 6 shows mass spectra for the data in the incident momentum interval 390 to 400 MeV/c for six bins of production cosine. The curves are from the fits described below.

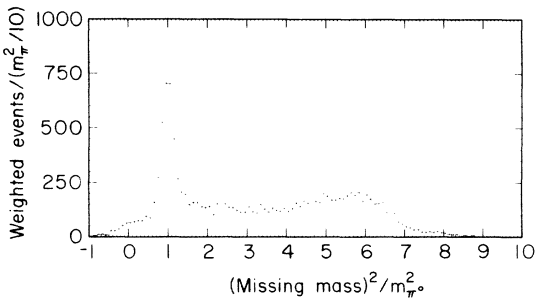

FIG. 5. Measured distribution of missing mass squared for events with incident momenta between 390 and 400 MeV/c.

IV. FITS TO THE DATA

In order to determine cross sections, angular distributions, and polarizations for the $\Sigma^0\pi^0$ and $\Lambda\pi^0$ final states a maximum-likelihood fit was made. The data were divided into intervals of 10 MeV/c and the data in each interval were fitted independently. The probability for each event was written as the sum of probabilities that the event was produced in one of the reactions above:

$$P(\mu_i{}^2, \cos\theta_i, \cos\beta_i) = p_{\Lambda\pi^0} + p_{\Sigma^0\pi^0} + p_{\Lambda\pi^0\pi^0} + \cdots .$$

We now describe the expressions used for each

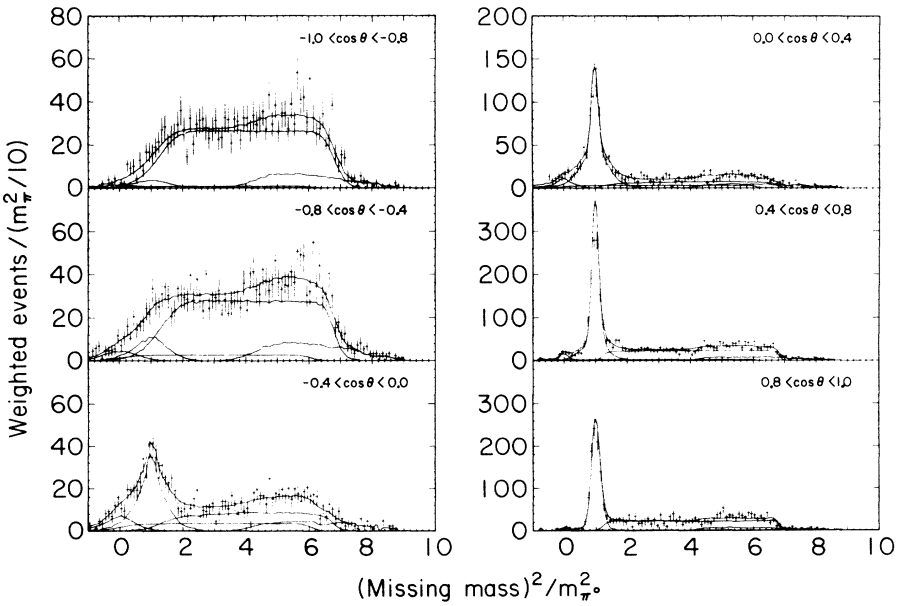

FIG. 6. Distributions in missing mass squared for data in the incident momentum interval 390 to 400 MeV/c for six bins of the missing mass production cosine. The curves are the contributions from different final states and the total derived from the fits described in the text.

of these probabilities. A Gaussian resolution function has been used to account for the finite resolution in μ^2,

$$R(\mu^2, \mu'^2) = \frac{1}{\sqrt{2\pi}\,\delta(\mu^2)} \exp\left[-\frac{1}{2}\left(\frac{\mu^2 - \mu'^2}{\delta(\mu^2)}\right)^2\right],$$

where the Gaussian width used for each event was the $\delta(\mu^2)$ calculated by SQUAW. The angular distributions and polarizations for the $\Sigma^0\pi^0$ and $\Lambda\pi^0$ have been expanded through $l = 4$.

The probability for the $\Lambda\pi^0$ final state is

$$P_{\Lambda\pi^0}(\mu^2, \cos\theta, \cos\beta) = f_{\Lambda\pi} R(\mu^2, m_\pi^2) \sum_{l=0}^{4} \left[\frac{A_l}{A_0} P_l(\cos\theta) + \alpha_\Lambda \cos\beta \sin\theta \frac{B_l}{A_0} P_l'(\cos\theta)\right],$$

where the Λ decay asymmetry parameter $\alpha = 0.645$ (Ref. 10). The parameter $f_{\Lambda\pi}$ is the fraction of the Λ + neutral events coming from $\Lambda\pi^0$ production. This fraction along with the A_l/A_0 and B_l/B_0 are varied in the fit.

The probability for the $\Sigma^0\pi^0$ final state is

$$P_{\Sigma^0\pi^0}(\mu^2, \cos\theta, \cos\beta) = f_{\Sigma\pi} \int_{\mu_{\min}^2}^{\mu_{\max}^2} R(\mu^2, \mu'^2) \sum_{l=0}^{4} \left[\frac{A_l}{A_0} U_l(\mu'^2) P_l(\cos\theta) + \alpha_\Lambda \cos\beta \sin\theta \frac{B_l}{A_0} V_l(\mu'^2) P_l'(\cos\theta)\right] d\mu'^2.$$

The functions U_l and V_l account for the spreading of the distribution due to decay of the Σ^0 into $\Lambda\gamma$. The forms of these functions are described in the Appendix. The computer code of this prescription for unfolding the Λ angular distribution and polarization to derive the Σ^0 angular distribution and polarization was tested to better than 1% in the coefficients using Monte Carlo generated events. The coefficients A_l and B_l, describing the $\Sigma^0\pi^0$ angular distribution and polarization in the K^-p rest frame, along with the fraction $f_{\Sigma\pi}$ are varied in the fits.

The probability for the $\Lambda\pi^0\pi^0$ final state is

$$P_{\Lambda\pi\pi}(\mu^2, \cos\theta, \cos\beta) = f_{\Lambda\pi\pi} \int g(\mu'^2, \cos\theta, \cos\beta) R(\mu^2, \mu'^2) d\mu'^2.$$

Only the fraction $f_{\Lambda\pi\pi}$ was varied in the fitting. The function g has been calculated from the results of a detailed analysis of the related channel $\Lambda\pi^+\pi^-$. An isobar model partial-wave analysis has been made of 9200 $\Lambda\pi^+\pi^-$ events from the same exposure, and the results have been published.[2] A good fit to the $\Lambda\pi^+\pi^-$ events was obtained with only six isobar amplitudes. The channel is dominated by $I = 0$ production of $\Sigma(1385)$ corresponding to the sequence $K^-p \to \Lambda(1520) \to \Sigma(1385)\pi \to \Lambda\pi^+\pi^-$; the isospin-1 production is very small. The $I = 0$ amplitudes found in the $\Lambda\pi^+\pi^-$ analysis contribute to $\Lambda\pi^0\pi^0$ and have been used to calculate the function g. The appropriate changes due to the $\pi^\pm - \pi^0$ mass difference were made.

The probability for the $\Lambda\gamma$ final state is

$$P_{\Lambda\gamma}(\mu^2, \cos\theta, \cos\beta) = f_{\Lambda\gamma} R(\mu^2, 0)[1 - \tfrac{1}{2}P_2(\cos\theta)].$$

A study of the reaction $K^-p \to \Lambda\gamma$ has been made from this same exposure.[9] By isolating a sample of events well resolved in μ^2 the cross section and angular distribution for the reaction were measured. The cross section peaks at 395 MeV/c, indicating dominance of $\Lambda(1520)$ production, and the angular distribution is consistent with $1 - \frac{1}{2}P_2(\cos\theta)$, expected from the electric dipole decay of $\Lambda(1520)$. In the fitting here both the angular distribution and the fraction $f_{\Lambda\gamma}$ were fixed. At 395 MeV/c the $\Lambda\gamma$ channel accounts for 2.4% of the Λ + neutral cross section:

$$P_{\Sigma^0\gamma} = 3.0\rho f_{\Lambda\gamma} \int_{\mu_{\min}^2}^{\mu_{\max}^2} R(\mu^2, \mu'^2) d\mu'^2 [1 - \tfrac{1}{2}P_2(\cos\theta)].$$

To describe the $\Sigma^0\gamma$ we have assumed that all the $\Lambda\gamma$ comes from $\Lambda(1520)$ and then used U-spin conservation to calculate $\Sigma^0\gamma$. U-spin invariance gives a factor 3 in cross section, ρ is the ratio of phase space (about 0.85), and we have neglected the spreading of the angular distribution from the Σ^0 decay. At 395 MeV/c, $\Sigma^0\gamma$ accounts for 6.2% of the Λ + neutrals cross section.

There is no direct way to measure the $\Lambda\pi\gamma$ and $\Sigma^0\pi^0\gamma$ contributions here. Estimates made on the basis of phase space arguments and SU(3), however, indicate they contribute about 0.1% of the cross section. We have neglected these in the fitting.

An analysis of the $\Sigma^+\pi^\mp\pi^0$ and $\Sigma^0\pi^+\pi^-$ final states has been made from data from this same exposure.[2] That analysis showed that the $\Sigma\pi\pi$ final states were dominated by $\Lambda(1520)$ production and were consistent with the decay sequence $\Lambda(1520) \to \Sigma(1385)\pi \to \Sigma\pi\pi$. However, isospin conservation prohibits the $\Sigma^0\pi^0\pi^0$ final state from this

sequence. A small amount of $\Sigma\pi\pi$ phase space was found in the charged channels, and this leads to an estimate of 0.2% $\Sigma^0\pi^0\pi^0$ in the Λ + neutral near 390 MeV/c incident momentum. We have neglected this in the fitting.

The variables μ^2 and $\delta(\mu^2)$ from SIOUX have been altered slightly before fitting the data. In the raw data a systematic shift in the mass of the π^0 peak was observed. Such a shift can arise from small systematic errors in the beam momentum, the fitted energy of the Λ, the production angle of the Λ, or the adjustment for bubble density (0.6mm) made to the observed K^-p interaction point. We have corrected the data with a phenomenological shift which varied from -0.08 m^2 at $\cos\theta = 0.0$ to $\cos\theta = \pm 1.0$. Introduction of this shift changed the fractions by ≤ 0.004 and the Legendre coefficients by less than $\frac{1}{2}$ standard deviation. The error $\delta(\mu^2)$ was scaled by a factor f_s for events with stopping protons and f_l for events with leaving protons. Variation of these scaling factors made a small improvement in the likelihood. The final fitting was made with $f_s = 1.2$ and $f_l = 1.0$. Inclusion of these scaling factors changed the Legendre coefficients by an average of 0.1 standard deviations and the fractions by 0.003.

Using the above expressions, a likelihood fit to the data was made using the OPTIME system.[11] The Legendre expansion coefficients and the fractions $f_{\Lambda\pi}$, $f_{\Sigma\pi}$, and $f_{\Lambda\pi\pi}$ were varied in the fits. Monte Carlo events with the same distribution of errors were used to plot the fits over the data for comparison. The curves resulting from the fit at 395 MeV are shown in Figs. 6(a) to 6(f). The data have been broken into six bins of Λ production cosine. The contributions from the individual channels as well as the total are drawn. The fits correctly reproduce the variations with incident momentum and production cosine.

The cross sections and coefficients from these fits were then corrected to take into account a systematic error introduced by beam-averaging the individual events in SQUAW. For each of the 24 beam settings an average beam momentum was established from the τ's and this average momentum was averaged with the measured momentum of the K^- track before kinematic fitting. This beam averaging procedure was done for both the Λ events and the τ's used to determine the pathlength. Since the τ's (3 constraint) were better constrained than the Λ's (0 constraint), the distribution in momentum for the Λ's was pulled closer to the average. This had the effect of artificially raising the cross section for momenta in the center of the distribution and lowering it on the sides. This artifact became apparent in comparing the cross sections from events from different beam settings. The experiment of Berley *et al.* that measured these channels in this momentum region also found cross sections and coefficients from different runs to be inconsistent (see Figs. 3 and 7–10). Using the known beam-averaging procedure and the known error distributions, we derived an algorithm for correcting the cross sections and Legendre coefficients.[12] The algorithm also included an unfolding of the uncertainty in the beam momentum. The algorithm was applied to the data and the resulting cross sections from different beam settings agreed well. The changes in the final cross sections averaged about one standard deviation and the changes in the coefficients averaged much less than a standard deviation. All of the results described in the following section have been corrected.

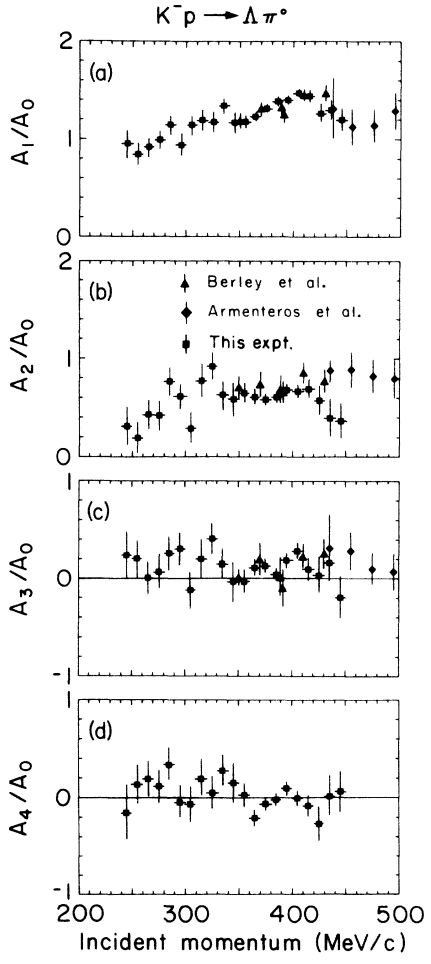

FIG. 7. Legendre coefficients A_l/A_0 ($l = 1$–4) as a function of incident momentum for the angular distribution in the reaction $K^-p \to \Lambda\pi^0$. The data of Berley *et al.* (Ref. 13) and Armenteros *et al.* (Ref. 14) are shown for comparison.

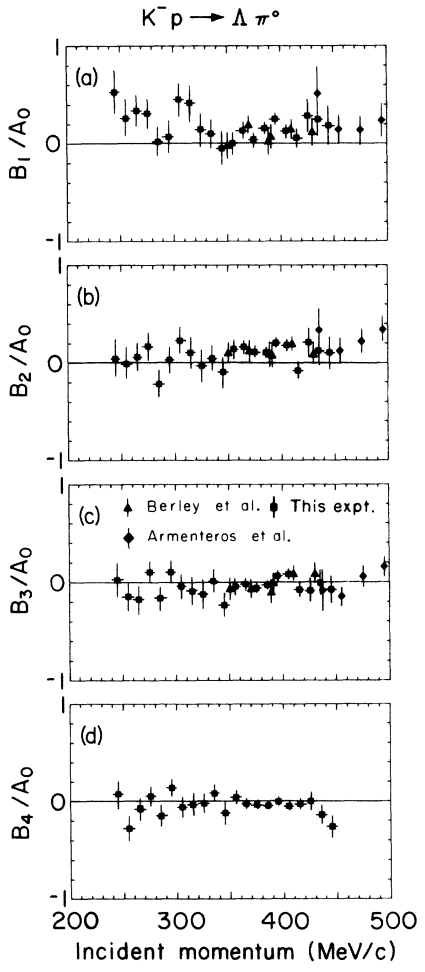

FIG. 8. Legendre coefficients B_l/A_0 ($l=1-4$) as a function of incident momentum for the Λ polarization in the reaction $K^-p \to \Lambda\pi^0$. The data of Berley *et al.* (Ref. 13) and Armenteros *et al.* (Ref. 14) are shown for comparison.

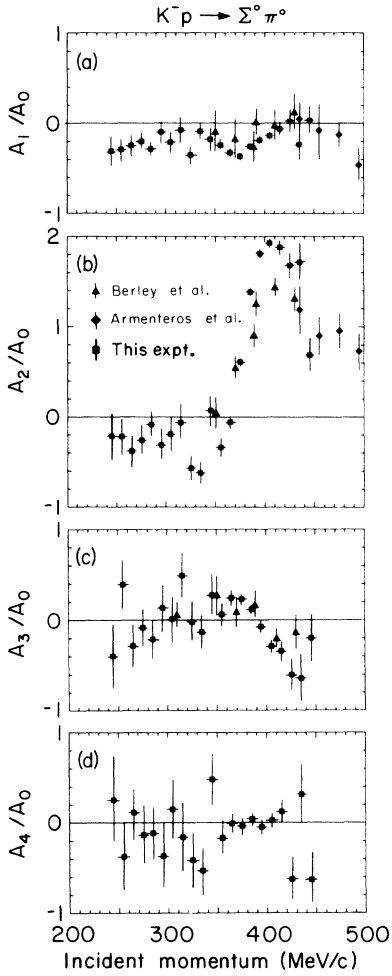

FIG. 9. Legendre coefficients A_l/A_0 ($l=1-4$) as a function of incident momentum for the angular distribution in the reaction $K^-p \to \Sigma^0\pi^0$. The data of Berley *et al.* (Ref. 13) and Armenteros *et al.* (Ref. 14) are shown for comparison.

V. RESULTS

The fractions $f_{\Lambda\pi}$, $f_{\Sigma\pi}$, and $f_{\Lambda\pi\pi}$ from the fits have been combined with the cross sections for all Λ + neutrals to derive the partial cross sections shown in Table I and Figs. 3(b), 3(c), and 3(d). The three cross sections are strongly correlated and only the diagonal errors are given in the table and the figures.

The $\Lambda\pi^0$ cross section [Fig. 3(b)] falls smoothly from about 10 mb at 245 MeV/c to about 3 mb at 445 MeV/c. Our data fall systematically below those of Berley *et al.*[13] and slightly above those of Watson *et al.*[1] in the region near $\Lambda(1520)$. At the upper end, our data connect smoothly with the results of Armenteros *et al.*[14] The $\Lambda(1520)$ has $I=0$ and the lack of structure near 400 MeV/c in this pure $I=1$ channel is evidence that the procedure described above has cleanly separated the final states.

The $\Sigma^0\pi^0$ cross section [Fig. 3c)] shows a marked peak from the $\Lambda(1520)$ of about 4 mb above a 3 mb background. There is no other significant structure. Again our data are systematically below those of Berley *et al.* and join smoothly with those of Armenteros *et al.*

The $\Lambda\pi^0\pi^0$ cross section [shown as full circles in Fig. 3(d)] rises rapidly from zero to 1.7 mb and then falls to about 1.0 mb. Although the forms of the $\Lambda\pi^0\pi^0$ mass spectra and angular distributions were fixed in the fitting, the amount of this channel was freely chosen by the fit. Isotopic spin invariance predicts the $\Lambda\pi^0\pi^0$ cross section is $\frac{1}{2}$ of the

$\Lambda\pi^+\pi^-$ cross section, since the latter is almost pure $I=0$.[2] Figure 3(d) shows as vertical lines the measured $\Lambda\pi^+\pi^-$ cross sections multiplied by 2ρ, where ρ is the ratio of available phase space. The excellent agreement is an additional consistency check on the separation of the different final states.

The Legendre coefficients for the $\Lambda\pi^0$ angular distribution and polarization are shown in Figs. 7 and 8 and Table II. Only the diagonal errors are shown. The A_1/A_0 is in agreement with both Berley *et al.* and Armenteros *et al.*, while the A_2/A_0 coefficient is in agreement with Berley and falls below the results of Armenteros at the upper end. A_3/A_0 is slightly positive and A_4/A_0 is consistent with zero. The B_1/A_0 and B_2/A_0 are both significantly nonzero and positive throughout this region and in agreement with the previous experiments[13,14]; B_3/A_0 and B_4/A_0 are consistent with zero.

The Legendre coefficients for the $\Sigma^0\pi^0$ angular distributions and polarizations are shown in Table III and Figs. 9 and 10. Both the A's and B's show dramatic behavior from the $\Lambda(1520)$ D wave and its interference with the dominant S-wave background. The data of Berley *et al.* show considerably less A_2/A_0 than our own.

The differential cross sections for π^0 production at 0° and 180° in the reactions $\Lambda\pi^0$ and $\Sigma^0\pi^0$ can be calculated from the Legendre coefficients and the total cross sections. These are displayed as a function of momentum in Fig. 11. Uncertainties are calculated using the full error matrix. The spectacular rise and fall of the $\Sigma^0\pi^0$ cross section in the vicinity of 390 MeV/c both at 0° and 180° is observed only slightly, if at all, in $\Lambda\pi^0$. Neither for forward produced Λ, where the missing mass is poorly measured, nor for backward produced Λ is there any evidence for more than a few percent contamination from $\Sigma^0\pi^0$, indicating once again the clean separation of these channels. Alternatively, any effect seen could also be ascribed to isospin impurity once suggested by Dalitz and Von Hippel[15] and investigated by Berley *et al.*[13]

Below 350 MeV/c the $\Sigma^0\pi^0$ cross sections in the forward and backward directions behave erratically, fluctuating well outside of their statistical uncertainty. We have no explanation for this. Perhaps it comes from the paucity of events below 350 MeV/c, inadequate for the elaborate parameterization. The $\Lambda\pi^0$ cross sections show no significant evidence for structure.

Interest in the region near 280 MeV/c incident momentum has been generated by an enhancement seen by Pan and Forman[16] in the reaction $\pi^+p \to K^+\pi^+\Lambda$. On the basis of an enhancement seen in the $\Lambda\pi^+$ mass distribution and structure in the polarization, they suggest an isotopic spin-1

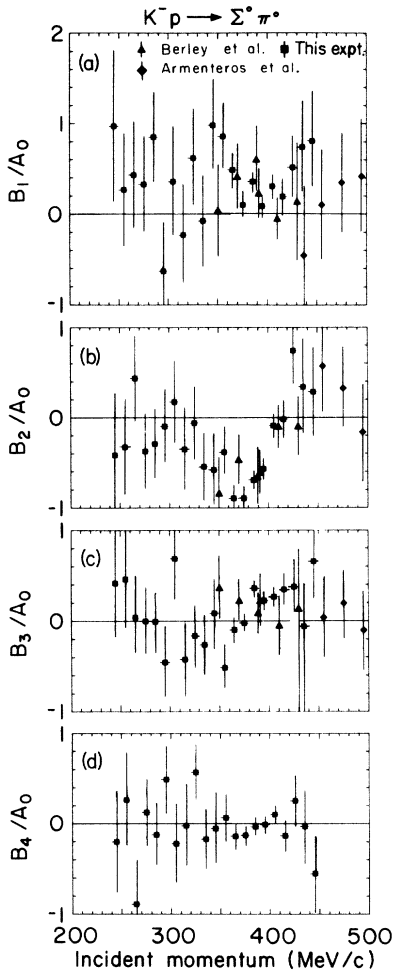

FIG. 10. Legendre coefficients B_l/A_0 ($l=1$–4) as a function of incident momentum for the Σ^0 polarization in the reaction $K^-p \to \Sigma^0\pi^0$. The data of Berley *et al.* (Ref. 13) and Armenteros *et al.* (Ref. 14) are shown for comparison.

resonance with mass = 1480 ± 15 MeV and width = 35 ± 20 MeV. Cline, Laumann, and Mapp[17] also suggest the possibility of a resonance with this mass. They observe in this energy region rapid variations in Legendre coefficients which describe the $\Lambda\pi^-$ angular distribution in the reaction $K^-d \to \Lambda\pi^-p$. However, the complications introduced by the three-particle final state in both these experiments make a clean resonance interpretation of these effects difficult.

In our experiment there is no statistically significant evidence for such a resonance at 1480 MeV, either in the $\Lambda\pi^0$ cross section of Fig. 3(b) or in the angular distribution and polarization data of Figs. 7, 8, 11(a), and 11(b). However, it should be emphasized that the bulk of our data lies at higher momenta and that our pathlength in this re-

TABLE I. Cross sections and errors (mb) for Λ + missing neutrals, $\Lambda\pi^0$, $\Sigma^0\pi^0$, and $\Lambda\pi^0\pi^0$ final states.

Momentum (MeV/c)	$\sigma(\Lambda$ + neutrals)	$\sigma(\Lambda\pi^0)$	$\sigma(\Sigma^0\pi^0)$	$\sigma(\Lambda\pi^0\pi^0)$
225	15.98 ± 2.84			
235	12.78 ± 1.60			
245	18.42 ± 1.60	10.23 ± 1.06	8.18 ± 0.92	
255	16.50 ± 1.14	8.82 ± 0.74	7.68 ± 0.68	
265	13.88 ± 0.86	7.77 ± 0.58	6.11 ± 0.50	
275	14.77 ± 0.85	8.04 ± 0.56	6.73 ± 0.50	
285	11.16 ± 0.63	5.56 ± 0.40	5.61 ± 0.40	
295	12.47 ± 0.71	6.69 ± 0.47	5.78 ± 0.43	
305	11.85 ± 0.67	6.35 ± 0.45	5.49 ± 0.41	
315	9.91 ± 0.60	5.29 ± 0.40	4.37 ± 0.36	0.21 ± 0.36
325	10.09 ± 0.56	5.41 ± 0.37	4.48 ± 0.33	0.14 ± 0.32
335	9.69 ± 0.53	5.22 ± 0.34	4.11 ± 0.30	0.26 ± 0.29
345	9.81 ± 0.52	4.78 ± 0.33	4.77 ± 0.33	0.10 ± 0.37
355	9.61 ± 0.33	4.86 ± 0.21	4.15 ± 0.19	0.33 ± 0.19
365	10.08 ± 0.25	4.21 ± 0.13	4.86 ± 0.15	0.54 ± 0.13
375	12.53 ± 0.24	4.29 ± 0.11	6.45 ± 0.15	0.97 ± 0.12
385	15.27 ± 0.25	4.20 ± 0.10	8.30 ± 0.15	1.53 ± 0.13
395	15.03 ± 0.27	3.96 ± 0.11	8.10 ± 0.16	1.66 ± 0.14
405	13.14 ± 0.30	3.90 ± 0.12	6.72 ± 0.17	1.52 ± 0.15
415	11.71 ± 0.29	3.87 ± 0.14	5.93 ± 0.18	1.20 ± 0.17
425	10.84 ± 0.36	4.05 ± 0.20	5.17 ± 0.22	1.10 ± 0.23
435	7.57 ± 0.41	3.49 ± 0.26	2.97 ± 0.24	0.71 ± 0.26
445	8.11 ± 0.54	3.45 ± 0.31	3.26 ± 0.30	1.08 ± 0.32
455	9.25 ± 0.71			
465	6.51 ± 0.58			

gion is only about 150 events/mb per 10 MeV/c. In order to expose a resonance of low elasticity, clearly more pathlength here would be desirable. Quantitatively, we may say that if a resonance of mass and width given by Ref. 16 were to have as much as 5% coupling to the $\bar{K}N$ channel and were to decay dominantly via $\Lambda\pi^0$, then we would observe a $3.7(J+\frac{1}{2})$ mb enhancement in the $\Lambda\pi^0$ cross section centered at 280 MeV/c with a full width of 100 MeV/c. A coupling this large to the elastic channel seems to be ruled out by the cross section data displayed in Fig. 3(b). Under further assumptions concerning the behavior of the nonresonant $\Lambda\pi^0$ amplitudes, more quantitative restrictions on such a resonance could be developed using also the angular distribution and polarization data in a partial-wave analysis of this channel.

The results presented here when combined with data at the corresponding momenta from the $\bar{K}N$ and $\Sigma^{\pm}\pi^{\mp}$ channels soon to become available from this experiment will permit a more detailed understanding of the partial waves contributing to the reactions than has heretofore been possible. An energy-dependent coupled-channel partial-wave analysis covering the 0–450 MeV/c momentum region and incorporating all the data from this experiment as well as data from other experiments at lower momenta will then be presented.[18]

APPENDIX

In the reaction $K^-p \to \Sigma^0\pi^0$, $\Sigma^0 \to \Lambda\gamma$ the angular distributions and polarization of the Λ can be measured and described in terms of Legendre polynomial expansions. In this appendix we describe the formulas used to relate the measured Legendre coefficients for the Λ to those describing the angular distribution and polarization of the Σ^0.

The relations used here are based on the work of Cha and Sucher.[19] We have converted their general expressions to relations between Legendre polynomial expansion coefficients.

Table IV and Fig. 12 define the notation used. Cha and Sucher derive the following distribution for the Λ [Eq. (2.14)]:

$$\frac{d\sigma}{dE_\Lambda d\cos\theta_\Lambda} = \frac{1}{2\pi(E_\Lambda^+ - E_\Lambda^-)} \int_0^{2\pi} \frac{d\sigma}{d\cos\gamma} d\phi . \quad \text{(A1)}$$

Expanding the production angular distribution we write

TABLE II. Legendre polynomial coefficients A_l/A_0 and B_l/A_0 for $K^-p \to \Lambda\pi^0$.

Momentum (MeV/c)	A_1/A_0	A_2/A_0	A_3/A_0	A_4/A_0
245	0.953 ± 0.143	0.309 ± 0.204	0.241 ± 0.243	−0.153 ± 0.279
255	0.847 ± 0.111	0.194 ± 0.163	0.204 ± 0.190	0.133 ± 0.199
265	0.918 ± 0.104	0.432 ± 0.146	0.005 ± 0.163	0.189 ± 0.180
275	0.995 ± 0.091	0.420 ± 0.137	0.065 ± 0.159	0.114 ± 0.168
285	1.148 ± 0.099	0.767 ± 0.146	0.261 ± 0.171	0.336 ± 0.173
295	0.938 ± 0.101	0.617 ± 0.139	0.304 ± 0.165	−0.049 ± 0.167
305	1.143 ± 0.097	0.292 ± 0.156	−0.122 ± 0.184	−0.072 ± 0.174
315	1.187 ± 0.111	0.761 ± 0.171	0.199 ± 0.199	0.194 ± 0.189
325	1.160 ± 0.104	0.903 ± 0.146	0.404 ± 0.168	0.047 ± 0.162
335	1.321 ± 0.081	0.610 ± 0.142	0.148 ± 0.163	0.269 ± 0.157
345	1.154 ± 0.107	0.569 ± 0.175	−0.035 ± 0.206	0.147 ± 0.196
355	1.141 ± 0.068	0.609 ± 0.100	−0.027 ± 0.120	0.025 ± 0.115
365	1.195 ± 0.046	0.567 ± 0.068	0.109 ± 0.082	−0.204 ± 0.079
375	1.254 ± 0.038	0.523 ± 0.059	0.125 ± 0.071	−0.062 ± 0.067
385	1.311 ± 0.036	0.536 ± 0.055	0.038 ± 0.067	−0.023 ± 0.065
395	1.372 ± 0.042	0.658 ± 0.065	0.185 ± 0.077	0.094 ± 0.076
405	1.435 ± 0.042	0.632 ± 0.069	0.280 ± 0.082	−0.007 ± 0.077
415	1.427 ± 0.061	0.679 ± 0.097	0.095 ± 0.116	−0.082 ± 0.109
425	1.267 ± 0.101	0.583 ± 0.148	0.037 ± 0.181	−0.268 ± 0.176
435	1.306 ± 0.108	0.409 ± 0.190	0.169 ± 0.216	0.013 ± 0.213
445	1.202 ± 0.110	0.372 ± 0.183	−0.195 ± 0.218	0.062 ± 0.216

Momentum (MeV/c)	B_1/A_0	B_2/A_0	B_3/A_0	B_4/A_0
245	0.531 ± 0.241	0.043 ± 0.204	0.027 ± 0.172	0.074 ± 0.135
255	0.261 ± 0.211	−0.008 ± 0.166	−0.148 ± 0.140	−0.278 ± 0.117
265	0.342 ± 0.173	0.062 ± 0.149	−0.175 ± 0.134	−0.079 ± 0.104
275	0.310 ± 0.160	0.171 ± 0.134	0.099 ± 0.113	0.053 ± 0.088
285	0.021 ± 0.166	−0.213 ± 0.140	−0.162 ± 0.117	−0.151 ± 0.099
295	0.070 ± 0.165	0.032 ± 0.139	0.105 ± 0.116	0.138 ± 0.098
305	0.454 ± 0.175	0.232 ± 0.145	−0.042 ± 0.124	−0.058 ± 0.100
315	0.412 ± 0.193	0.103 ± 0.170	−0.090 ± 0.148	−0.034 ± 0.107
325	0.143 ± 0.172	−0.030 ± 0.169	−0.123 ± 0.149	−0.019 ± 0.105
335	0.097 ± 0.155	0.047 ± 0.128	0.012 ± 0.116	0.084 ± 0.083
345	−0.050 ± 0.184	−0.096 ± 0.156	−0.231 ± 0.128	−0.119 ± 0.110
355	−0.000 ± 0.116	0.134 ± 0.099	−0.043 ± 0.084	0.043 ± 0.065
365	0.132 ± 0.079	0.158 ± 0.068	−0.022 ± 0.059	−0.023 ± 0.046
375	0.037 ± 0.068	0.108 ± 0.058	−0.057 ± 0.050	−0.041 ± 0.038
385	0.152 ± 0.060	0.098 ± 0.052	−0.023 ± 0.045	−0.044 ± 0.035
395	0.246 ± 0.068	0.203 ± 0.059	0.063 ± 0.050	−0.002 ± 0.041
405	0.125 ± 0.073	0.174 ± 0.063	0.084 ± 0.054	−0.048 ± 0.042
415	0.053 ± 0.102	−0.077 ± 0.089	−0.073 ± 0.075	−0.028 ± 0.057
425	0.288 ± 0.167	0.211 ± 0.145	−0.087 ± 0.122	0.002 ± 0.092
435	0.254 ± 0.185	0.128 ± 0.156	−0.005 ± 0.137	−0.139 ± 0.099
445	0.186 ± 0.205	0.104 ± 0.166	−0.070 ± 0.141	−0.261 ± 0.106

$$\frac{d\sigma}{d\cos\gamma} = \sum_{l=0}^{\infty} A_l P_l(\cos\gamma)\,. \tag{A2}$$

Using the vector addition theorem, $P_l(\cos\gamma)$ can be expressed as

$$P_l(\cos\gamma) = P_l(\cos\chi)P_l(\cos\theta_\Lambda) + 2\sum_{m=1}^{l}\frac{(l-m)!}{(l+m)!}P_l^m(\cos\chi)P_l^m(\cos\theta_\Lambda)\cos m\phi\,. \tag{A3}$$

TABLE III. Legendre polynomial coefficients A_l/A_0 and B_l/A_0 for $K^-p \to \Sigma^0\pi^0$.

Momentum (MeV/c)	A_1/A_0	A_2/A_0	A_3/A_0	A_4/A_0
245	−0.313 ± 0.173	−0.215 ± 0.253	−0.398 ± 0.350	0.251 ± 0.488
255	−0.293 ± 0.138	−0.218 ± 0.193	0.396 ± 0.263	−0.373 ± 0.395
265	−0.248 ± 0.118	−0.379 ± 0.174	−0.283 ± 0.226	0.116 ± 0.287
275	−0.205 ± 0.108	−0.260 ± 0.155	−0.087 ± 0.216	−0.135 ± 0.325
285	−0.286 ± 0.105	−0.085 ± 0.148	−0.211 ± 0.204	−0.115 ± 0.292
295	−0.099 ± 0.124	−0.317 ± 0.181	0.133 ± 0.263	−0.370 ± 0.368
305	−0.211 ± 0.126	−0.195 ± 0.185	0.010 ± 0.243	0.146 ± 0.340
315	−0.074 ± 0.149	0.039 ± 0.210	0.482 ± 0.267	−0.156 ± 0.365
325	−0.346 ± 0.100	−0.535 ± 0.138	−0.018 ± 0.203	−0.406 ± 0.303
335	−0.090 ± 0.097	−0.580 ± 0.129	−0.131 ± 0.186	−0.516 ± 0.255
345	−0.178 ± 0.123	−0.064 ± 0.175	0.270 ± 0.228	0.471 ± 0.295
355	−0.234 ± 0.077	−0.249 ± 0.107	0.055 ± 0.138	−0.163 ± 0.185
365	−0.317 ± 0.046	0.281 ± 0.064	0.236 ± 0.083	−0.008 ± 0.110
375	−0.354 ± 0.039	0.551 ± 0.050	0.222 ± 0.064	−0.040 ± 0.087
385	−0.248 ± 0.035	1.315 ± 0.040	0.113 ± 0.054	0.037 ± 0.072
395	−0.187 ± 0.042	1.781 ± 0.046	−0.074 ± 0.063	−0.050 ± 0.084
405	−0.135 ± 0.046	1.877 ± 0.050	−0.283 ± 0.068	0.023 ± 0.088
415	−0.066 ± 0.072	1.859 ± 0.079	−0.344 ± 0.110	0.120 ± 0.138
425	0.027 ± 0.124	1.690 ± 0.133	−0.608 ± 0.180	−0.630 ± 0.246
435	−0.245 ± 0.179	1.747 ± 0.199	−0.652 ± 0.268	0.321 ± 0.341
445	0.029 ± 0.149	0.697 ± 0.184	−0.203 ± 0.254	−0.633 ± 0.306

Momentum (MeV/c)	B_1/A_0	B_2/A_0	B_3/A_0	B_4/A_0
245	0.969 ± 0.853	−0.418 ± 0.695	0.415 ± 0.600	−0.203 ± 0.570
255	0.264 ± 0.641	−0.324 ± 0.536	0.458 ± 0.530	0.262 ± 0.523
265	0.428 ± 0.601	0.433 ± 0.483	0.042 ± 0.461	−0.892 ± 0.468
275	0.323 ± 0.535	−0.376 ± 0.428	−0.001 ± 0.383	0.126 ± 0.384
285	0.850 ± 0.500	−0.290 ± 0.383	−0.007 ± 0.334	−0.125 ± 0.349
295	−0.632 ± 0.536	−0.098 ± 0.417	−0.453 ± 0.395	0.489 ± 0.383
305	0.357 ± 0.623	0.176 ± 0.473	0.686 ± 0.437	−0.223 ± 0.443
315	−0.232 ± 0.571	−0.344 ± 0.458	−0.421 ± 0.419	−0.024 ± 0.472
325	0.604 ± 0.549	−0.056 ± 0.407	−0.161 ± 0.354	0.556 ± 0.319
335	−0.076 ± 0.508	−0.532 ± 0.379	−0.257 ± 0.331	−0.172 ± 0.341
345	0.963 ± 0.507	−0.569 ± 0.417	0.083 ± 0.392	−0.054 ± 0.397
355	0.815 ± 0.370	−0.367 ± 0.290	−0.491 ± 0.256	0.064 ± 0.258
365	0.467 ± 0.205	−0.863 ± 0.160	−0.094 ± 0.144	−0.135 ± 0.146
375	0.095 ± 0.145	−0.853 ± 0.123	−0.022 ± 0.112	−0.126 ± 0.110
385	0.341 ± 0.108	−0.664 ± 0.103	0.348 ± 0.089	−0.033 ± 0.089
395	0.082 ± 0.120	−0.564 ± 0.121	0.220 ± 0.101	−0.009 ± 0.101
405	0.298 ± 0.135	−0.086 ± 0.139	0.261 ± 0.115	0.099 ± 0.109
415	0.190 ± 0.203	−0.018 ± 0.209	0.342 ± 0.170	−0.136 ± 0.169
425	0.518 ± 0.352	0.743 ± 0.377	0.376 ± 0.310	0.257 ± 0.274
435	0.750 ± 0.504	0.346 ± 0.534	−0.062 ± 0.449	−0.032 ± 0.416
445	0.816 ± 0.550	0.286 ± 0.496	0.660 ± 0.400	−0.560 ± 0.418

The integral over ϕ of the second term vanishes, yielding

$$\frac{d\sigma}{dE_\Lambda\, d\cos\theta_\Lambda} = \frac{1}{(E_\Lambda^+ - E_\Lambda^-)} \sum_{l=0}^{\infty} A_l P_l(\cos\chi) P_l(\cos\theta_\Lambda) . \tag{A4}$$

$\cos\chi$ is related to the energies of the Σ and Λ by

$$\cos\chi = \frac{2E_\Lambda E_\Sigma - m_\Sigma{}^2 - m_\Lambda{}^2}{2|p_\Sigma|\,|p_\Lambda|} . \tag{A5}$$

The missing neutral mass is given by

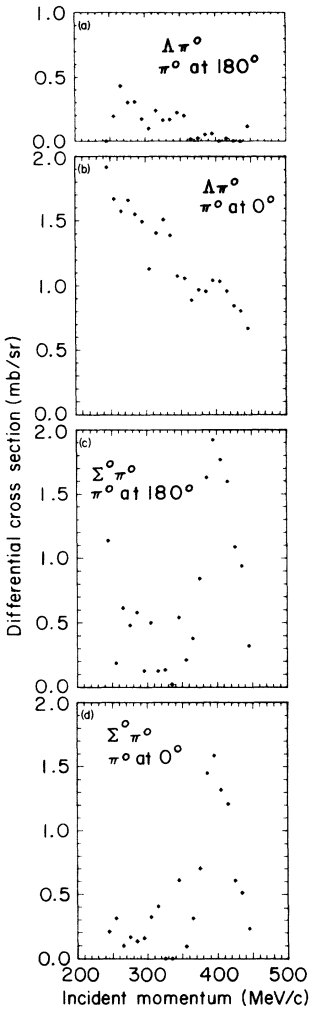

FIG. 11. Differential cross sections (mb/sr) at 0° and 180° for the reactions $K^-p \to \Lambda\pi^0$ (a), (b) and $K^-p \to \Sigma^0\pi^0$ (c), (d).

$$\mu^2 = E_{\text{c.m.}} - 2E_{\text{c.m.}}E_\Lambda + m_\Lambda{}^2 ,$$

and the differential cross section for the Λ becomes

$$\frac{d\sigma}{d\mu^2\, d\cos\theta_\Lambda} = \frac{1}{\mu_{\max}{}^2 - \mu_{\min}{}^2} \sum_{l=0}^{\infty} A_l P_l(\cos\chi) P_l(\cos\theta_\Lambda)$$

or

$$\frac{d\sigma}{d\mu^2\, d\cos\theta_\Lambda} = \sum_{l=0}^{\infty} A_l U_l(\mu^2) P_l(\cos\theta_\Lambda) , \tag{A6}$$

where

$$U_l(\mu^2) = \frac{1}{\mu_{\max}{}^2 - \mu_{\min}{}^2} P_l(\cos\chi) . \tag{A7}$$

Cha and Sucher's result relating the polarization of the Λ to that of the Σ^0 is the following:

$$\eta_\Lambda(\theta_\Lambda, E) = 2\pi \sin\theta_\Lambda\, \xi_\Lambda \Big/ \int_0^{2\pi} \frac{d\sigma}{d\cos\gamma} d\phi ,$$

where

$$\xi_\Lambda = \frac{1}{2\pi} \alpha_0 |\vec{p}_\Lambda| |\vec{p}_\Sigma| \sin^2\chi \int_0^{2\pi} \xi_\Sigma(\cos\gamma) \sin^2\phi\, d\phi .$$

(A8)

η_Λ is the polarization of the Λ in the direction

$$\frac{\vec{p}_K \times \vec{p}_\Lambda}{|\vec{p}_K \times \vec{p}_\Lambda|} \text{ and } \alpha_0 = \frac{-4 m_\Sigma m_\Lambda}{(m_\Sigma - m_\Lambda)^2} .$$

ξ_Σ is related to the polarization of the Σ^0, η_Σ by

$$\eta_\Sigma = \sin\theta_\Sigma\, \xi_\Sigma \Big/ \frac{d\sigma}{d\cos\gamma} . \tag{A9}$$

We expand IP for the Σ^0 as follows:

$$IP = \frac{d\sigma}{d\cos\gamma} \eta_\Sigma = \sin\gamma \sum_{l=1}^{\infty} B_l P_l{}'(\cos\gamma) . \tag{A10}$$

TABLE IV. Notation used in the description of $K^-p \to \Sigma^0\pi^0$, $\Sigma^0 \to \Lambda\gamma$. All quantities listed here are defined in the K^-p center-of-mass system. The Λ momentum is chosen along the z axis and the beam is chosen in the x-z plane. See Fig. 12.

θ_Λ	the polar angle of the beam with respect to the Λ
$\chi\ \phi$	the polar and azimuthal angles of the Σ^0 with respect to the Λ
γ	the angle between the Σ^0 and the K^-
E_Λ, P_Λ	the energy and momentum of the Λ
E_Σ, p_Σ	the energy and momentum of the Σ^0
E_Λ^+, E_Λ^-	the maximum and minimum possible energy of the Λ

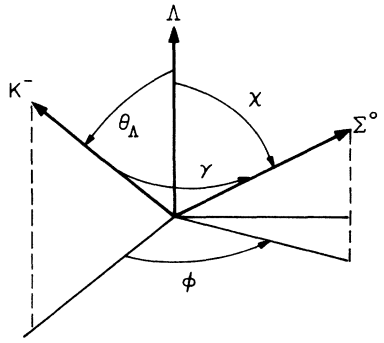

FIG. 12. Diagram defining the angles used in the analysis of the reaction $K^-p \to \Sigma^0\pi^0$, $\Sigma^0 \to \Lambda\gamma$.

TABLE V. Integrals of U_l and V_l over all missing mass. U_l and V_l are factors relating the Legendre coefficients which describe the angular distribution and polarization of the Σ^0 to those of the measured Λ.

Incident K^- momentum (MeV/c)	U_l				V_l			
	$l=1$	2	3	4	1	2	3	4
305	0.962	0.890	0.787	0.661	0.325	0.311	0.290	0.263
345	0.966	0.901	0.807	0.692	0.326	0.313	0.294	0.270
385	0.970	0.910	0.826	0.720	0.327	0.315	0.298	0.276
425	0.973	0.919	0.842	0.746	0.327	0.317	0.301	0.281
465	0.975	0.927	0.857	0.768	0.328	0.318	0.304	0.286

Thus

$$\eta_\Lambda(\theta_\Lambda, E_\Lambda) = \sin\theta_\Lambda\, \alpha_0 |\vec{p}_\Lambda||\vec{p}_\Sigma| \sin^2\chi \times \sum_{l=1}^{\infty} B_l I_l \Big/ \int_0^{2\pi} \frac{d\gamma}{d\cos\gamma} d\phi ,$$

where

$$I_l = \int_0^{2\pi} P_l(\cos\gamma)\sin^2\phi\, d\phi . \tag{A11}$$

Now, using the relation

$$\cos\gamma = \cos\chi\cos\theta_\Lambda - \sin\chi\sin\theta_\Lambda\cos\phi \tag{A12}$$

and an integration by parts, I_l may be reexpressed as

$$I_l = -\int_0^{2\pi} \frac{P_l(\cos\gamma)\cos\phi\, d\phi}{\sin\theta_\Lambda \sin\chi} .$$

Application of the vector addition theorem yields

$$I_l = 2\pi \frac{(l-1)!}{(l+1)!} P_l'(\cos\theta_\Lambda) P_l'(\cos\chi) . \tag{A13}$$

Now, with relations (A6), (A7), (A11), and (A13) for the angular distributions and polarization we can express the measured distribution as

$$\frac{d\sigma}{d\mu^2\, d\cos\theta_\Lambda\, d\cos\beta_\Lambda} = \sum_{l=0}^{\infty} A_l U_l P_l(\cos\theta_\Lambda) + \alpha_\Lambda \cos\beta \sin\theta_\Lambda \times \sum_{l=1}^{\infty} B_l V_l P_l'(\cos\theta_\Lambda) , \tag{A14}$$

where

$$U_l = \frac{1}{\mu_{\max}^2 - \mu_{\min}^2} P_l(\cos\chi) \tag{A15}$$

and

$$V_l = \frac{2\pi}{\mu_{\max}^2 - \mu_{\min}^2} \alpha_0 |\vec{p}_\Lambda||\vec{p}_\Sigma| \sin^2\chi \frac{P_l'(\cos\chi)}{l(l+1)} . \tag{A16}$$

α_Λ is the Λ decay asymmetry parameter and β is the angle between the Λ and the decay proton in the Λ rest frame.

These expressions for U_l and V_l can be integrated over the full range of μ^2 to give factors describing the smearing of the Σ^0 distribution (for all μ^2) by the decay. These integrals have been performed numerically and the results are shown in Table V for incident K^- momenta from 275 to 465 MeV/c.

*This work was performed under the auspices of the U. S. Atomic Energy Commission.

[1]M. B. Watson, M. Ferro-Luzzi, and R. D. Tripp, Phys. Rev. 131, 2248 (1963).

[2]Analyses of the $\Lambda\pi^+\pi^-$ and $\Sigma\pi\pi$ final states have been published in T. S. Mast *et al.*, Phys. Rev. D 7, 5 (1973); 7, 3212 (1973). Analyses of the $\Sigma^\pm\pi^\pm$ and $\bar{K}N$ final states are in progress.

[3]R. Bangerter, T. Mast, and R. Tripp (unpublished).

[4]R. O. Bangerter, Lawrence Berkeley Laboratory, Alvarez Group Physics Note No. 574, 1965 (unpublished).

[5]Most of the pathlength below 300 MeV/c is derived from an exposure of the 25-in. hydrogen bubble chamber to the same beam by Chan and Kadyk [see J. H. Chan, Lawrence Berkeley Laboratory Report No. LBL-350, 1971 (unpublished)].

[6]T. S. Mast, L. K. Gershwin, M. Alston-Garnjost, R. O. Bangerter, A. Barbaro-Galtieri, J. J. Murray, F. T. Solmitz, and R. D. Tripp, Phys. Rev. 183, 1200 (1969).

[7]S. E. Derenzo and R. H. Hildebrand, Nucl. Instrum. Methods 69, 287 (1969).

[8]R. Bangerter and T. Mast, Lawrence Berkeley Laboratory Alvarez Group Physics Note No. 731, 1971 (unpublished).

[9]T. S. Mast, M. Alston-Garnjost, R. O. Bangerter, A. Barbaro-Galtieri, L. K. Gershwin, F. T. Solmitz, and R. D. Tripp, Phys. Rev. Lett. 21, 1715 (1968).

[10]Particle Data Group, Rev. Mod. Phys. 43, S1 (1971).

[11]P. H. Eberhard and W. O. Koellner, Lawrence Berkeley Laboratory Reports Nos. UCRL-20159, 1970 (unpub-

lished) and UCRL-20160, 1971 (unpublished).
[12]R. Bangerter, Alvarez Group Physics Note (unpublished).
[13]D. Berley, S. P. Yamin, R. R. Kofler, A. Mann, G. W. Meisner, S. S. Yamamoto, J. Thompson, and W. Willis, Phys. Rev. D 1, 1996 (1970).
[14]R. Armenteros, P. Baillon, C. Briceman, M. Ferro-Luzzi, E. Pagiola, J. O. Petersen, D. E. Plane, N. Schmitz, E. Burkhardt, H. Filthuth, E. Kluge, H. Oberlack, R. R. Ross, R. Barloutaud, P. Granet, J. Meyer, J. P. Porte, and J. Prevost, Nucl. Phys. B21, 15 (1970).
[15]R. H. Dalitz and F. von Hippel, Phys. Lett. 10, 153 (1964).
[16]Y. Pan and F. Forman, Phys. Rev. Lett. 23, 806 (1969).
[17]D. Cline, R. Laumann, and J. Mapp, Nuovo Cimento Lett. 6, 205 (1972).
[18]Error matrices for the cross sections and Legendre coefficients presented here will be found in T. S. Mast *et al.*, LBL Report No. LBL-3853 (unpublished).
[19]M. H. Cha and J. Sucher, Phys. Rev. 140, 668 (1965).